sciendo

Civil and Environmental Engineering
Vol. 17, Issue 2, 500-512, DOI: 10.2478/cee-2021-0052

ANALYSIS OF GEOGRID REINFORCED STRUCTURES WITH A PASSIVE FACING SYSTEM USING DIFFERENT COMPUTATIONAL METHODS

Monika SULOVSKA[1,*], Jakub STACHO[1]

[1] Department of Geotechnics, Faculty of Civil Engineering, Slovak University of Technology in Bratislava, Radlinskeho 11, 810 05 Bratislava, Slovakia.
[*] corresponding author: monika.sulovska@stuba.sk

Abstract

The article deals with designing and analysing a wrapped geogrid reinforced structure (GRS) with a passive facing system. The analysis has been done using analytical calculation and numerical modelling. The analytical calculations were executed using FINE Geo5 geotechnical software, and numerical modelling was executed using Plaxis 2D software. The analysis is focused mainly on comparing tension forces in geogrids and the stability of the reinforced embankment determined using both computational methods. The deformation analysis was done only using numerical modelling. The numerical modelling allowed for a more detailed analysis of the wrapped GRS. Each construction phase was modelled step by step according to an actual construction procedure. Two complex road embankments supported by GRS were modelled and analysed. The first model consisted of three GRS, which not affected each other. In the second model, the GRS at each side of the embankment influenced each other. The analysis results showed that tension forces in geogrids, determined using both computational methods, can differ significantly from each other. The stability of the reinforced embankment determined using numerical modelling was within the range of 0.87 - 1.22 of the stability determined using analytical calculation. The numerical modelling results showed that the final horizontal deformation of the passive facing is about 2.8 - 3.8 times smaller than the deformation of the wrapped GRS, which occurs during the construction of the embankment.

Keywords:

Geogrid reinforced structure;
Wrapped facing;
Passive earth system facing;
Reinforced earth structure;
Mechanically stabilized earth wall.

1 Introduction

Geogrid reinforced earth structures (GRS) have been used for different types of earthworks, such as reinforced road and railway embankments, reinforced walls and abutments, reinforced soil layers below spread foundation, for over 40 years. The geosynthetic material allows the transferring of tensile forces in the earth structure through friction with the soil. In suitable conditions, the design of the GRS can lead to a more effective, economical and less time-consuming alternative than conventional methods. At present, there are several types and methods of construction of the GRS, see, e.g. [1, 2]. The facing type is an important characteristic of a GRS. It can be designed using different methods and materials, such as concrete blocks, gabions, steel mesh, and geogrid. The facing type has an impact on the magnitude and shape of deformations and global stability. The article is focused on wrapped GRS structure, where the geogrid is on the face side returned back into the soil/embankment, see, e.g. [3]. Depends on the facing technique, the wrapped GRS can be divided into two categories, i.e., active and passive facing system; the differences were published by, e.g. [4]. The wrapped GRS analyzed were constructed using a passive facing system. In this system, the wrapped GRS is built to a total height in the first step. An independent facing system giving the final form of the structure is constructed in the second/following step.

The current analytical calculation models are usually adapted for traditional retaining structures and do not enough consider characteristics and behaviour of reinforced soil, e.g. [5]. The analytical models are mostly based on the conventional soil mechanics theory [6]. The methods are very conservative in determining the tension forces in geogrids and deformations of GRS, see, e.g. [7]. Based on the case studies and tests results, different improvements and modifications of existing theories were adopted in analytical and empirical calculation models, e.g. [8]. The simplified semi-empirical calculation for determining the horizontal deformation of wrapped GRS was presented by, e.g. [9].

A successful design of geogrid reinforced earth structure can be achieved using numerical modelling, mostly by the finite element method (FEM). The numerical modelling allows for detailed and complex analysis of the GRS behaviour. The numerical analyses of GRS were published by, e.g. [10, 11]. At present, there are also advanced numerical methods, such as distinct-element modelling, allowing for modelling individual grains; however, they can analyse only a part of the structure due to their heavy requirements on computer hardware [12].

The in-situ testing and monitoring can be assumed as the most precise method to determine deformations of GRS. The most used methods are, e.g., inclinometer measurements or measurements using fibre optics, see, e.g. [13]. The monitoring of the wrapped GRS using more advanced technologies such as terrestrial laser scanner was published by [3]. The field tests and monitoring of wrapped GRS were presented by, e.g. [14]. The results showed that the ratios of maximum construction to maximum post-construction deformation could reach the ratio of about 4:1, which means that the greatest deformations are achieved during the construction. The monitoring and in situ testing is usually based on monitoring the facing deformations or deformations in preselected points and do not allow for detailed analyses focused on the behaviour of the GRS during the construction. It can be better done using laboratory tests on a small scale, e.g. [15], or large/real scale, see, e.g. [16]. While in the case of the small models, the interpretation of the results to the real scale can be difficult, in the real-scale models, the GRS modelled has limited dimensions.

The combination of numerical modelling and results of some tests, allowing the calibration of the numerical model, can lead to achieving the most relevant design approach. In Slovakia, the wrapped GRS are mostly designed using GEO5 software based on simple analytical approaches, or numerical modelling (FEM), usually using Plaxis software. The design of the two complex road embankments supported by wrapped GRS using both calculation methods is presented and analysed.

2 Construction of wrapped GRS with a passive facing system

In the initial phase of the construction, the surface of the original terrain is adapted to the construction of the embankment. The concrete strips (below the sides of the embankment) on a compacted gravel base are created. The construction of wrapped GRS involves the sequence of filling and laying geogrid reinforcement. During backfilling and compaction, the facing of wrapped GRS requires a support system, i.e. full-height formwork, layer by layer formwork, or permanent facing support (e.g. steel mesh) [3, 17]. The wrapped GRS presented have been constructed using layer by layer formwork. A connecting geogrid that will connect wrapped GRS body and facing blocks is inserted between each geogrid layer in a passive facing system. After the main body of the wrapped GRS is constructed to a total height, a passive facing system is constructed step by step. The facing blocks are usually placed 0.3 m from the wrapped GRS facing. A space between them is filled using compacted gravel. The facing blocks are connected with a wrapped GRS using the activation of connecting geogrids. This technique causes that relatively greater horizontal deformations of wrapped GRS body are “hidden”. The final deformations of the embankment are given only by secondary deformations of the passive facing system.

3 Calculation methods used and creating geotechnical models

GEO5 geotechnical software is based on simple analytical calculation models and allows for verification of an internal and global stability of the GRS and the vertical settlement of the embankment. Analytical approach allowing determination of horizontal deformation of the GRS has been not implemented in the software yet. The geogrids are designed to the forces determined by internal stability calculation. Determination of forces is performed by dividing the calculated active earth pressure into individual layers. Each geogrid transmits a part of the active pressure, which acts on the respective layer. A linear shape of the shear surface for flexible geogrids is considered [18]. The embankment settlement can be determined using the analytical approach, which considers

oedometer conditions (according to STN 73 1001: Geotechnical structures, Foundation: 2010); stated by, e.g. [19]. Global stability can be verified using different methods. Depend on the boundary conditions of the analysed embankments; two calculation methods were used, i.e., Bishop's method with the circular slip surface, and Sarma's method with polygonal slip surface, see, e.g. [18].

Plaxis geotechnical software is based on the finite element method (FEM) and allow for a more detailed and complex analysis of the behaviour of the wrapped GRS. The models were created as plane strain models using triangular 15-node elements. The mesh of finite elements was refined especially close to the facing of the wrapped GRS to obtain its adequate deformation. The model had standard fixities [20]. Soils were modelled using the Hardening Soil (HS) material model [21]. Fine-grained soils were modelled as the A-type undrained and coarse-grained soils were modelled as drained [20]. The concrete strips and facing blocks were modelled using the Linear Elastic (LE) material model. The wearing course of a road was modelled using the elastic plate; properties are stated in Table 1. The geogrid was modelled using elastoplastic isotropic geogrid material type. Elastic stiffness $E_{geogrid} \cdot A_{geogrid}$ was given by geogrids area $A_{geogrid}$ and elastic modulus of the material $E_{geogrid}$, averaged per meter width. The plastic threshold N_p was applied. Two main geogrids were used in embankments analysed, i.e., Huesker Fortrac MP80/25-20/30 (MP80) and Huesker Fortrac 110/25-20/30 (MP110); properties are stated in Table 1. A standard interface was taken into account between geogrids and soils, see, e.g., [20]. The property of the interface is given by R_{inter} parameter [20]. Mirmoradi and Ehrlich [22] suggest rigid interface for soil-geogrid interaction, i.e. R_{inter} = 1.0. Drusa et al. [23] stated that R_{inter} parameter could be directly set in the soil, based on practical experiences, see also [20], and a value of 0.9 for crushed stone material can be used. Based on the results of the laboratory tests presented by Stacho et al. [24], the R_{inter} parameter for the material of analysed embankments (Tables 3 and 4) exceed the value of 1.0; so in numerical models, R_{inter} = 1.0 was used.

Table 1: Selected properties of geogrids and materials used.

Geogrids			
Parameter [unit]	**Fortrac**		**Thrace**
	R80/25-20/30MPT	**R110/25-20/30MPT**	**TG4545S**
$E_{geogrid} \cdot A_{geogrid}$ - Axial stiffness [kNm^{-1}]	1100	1650	750
N_p [1)] - Short-time tension strength: T_{ult} [kNm^{-1}]	80	110	45
N_p [2)] - Long-time tension strength: R_t [kNm^{-1}]	43.54	65.07	26.62
Other materials			
Material	**Parameter [unit]**		
	γ[kNm^{-3}]	**E [MNm^{-2}]**	**ν[-]**
Facing block	19	100	0.3
Concrete	23	35000	0.2

Two road embankments supported by wrapped GRS with a passive facing system were modelled and analysed. Model 1 represents a wide embankment with a complex geometry, where, as can be estimated, the wrapped GRS do not affect each other. The geometry of the embankment and the placing and marking of the geogrids are shown in Fig. 1. The load from traffic was modelled according to Load Model 1 (LM1) of Eurocode 1: Actions on structures. Part 2: Traffic loads on bridges: 2006; see Table 2. The LM1 acting the left road (top of the embankment) was applied from left to right, and the LM1 acting the right road was applied from right to left. The LM1 acting the 8 m width road, which has the surface at +2.33 m (Fig. 1), was also applied from right to left. The coefficients which define the road category $\alpha_{Q,i}$ and $\alpha_{q,i}$; were selected for a motorway, Table 2.

Table 2: Application of the load based on LM1.

Loading		**Width of the lane**	**TS (Tandem System)**	**UDL (Uniformly Distributed Load)**	**Coefficients for a road category**	
Marking (Unit)		**[m]**	**$Q_{i,k}$ [kN]**	**$q_{i,k}$ [kNm^{-2}]**	**$\alpha_{Q,i}$ [-]**	**$\alpha_{q,i}$ [-]**
Location	Lane No.1	3	300	9.0	0.9	0.9
	Lane No.2	3	200	2.5	0.9	1
	Lane No.3	3	100	2.5	0.9	1
	Remaining area	-	-	2.5	-	1

The properties of the embankment material, gravel silty, are presented in Table 3. The subsoil consisted of thin layers of quaternary soils, such as clay of intermediate plasticity, sandy silt/clay, or sand and gravel with fine content, respectively, to a depth of 8.5 m below the surface. Below the quaternary soils, there were the neogene soils, such as clayey sand/gravel and clay of intermediate to high plasticity. The groundwater level was about 2.9 m below the terrain level. The properties of soils used in calculations are presented in Table 3. While analytical calculations did not allow the construction progress to be taken into account, numerical modelling took into account 48 construction phases, Table 5. The construction phases were modelled as consolidation phases with estimated construction times because of consolidation of fine-grained subsoil.

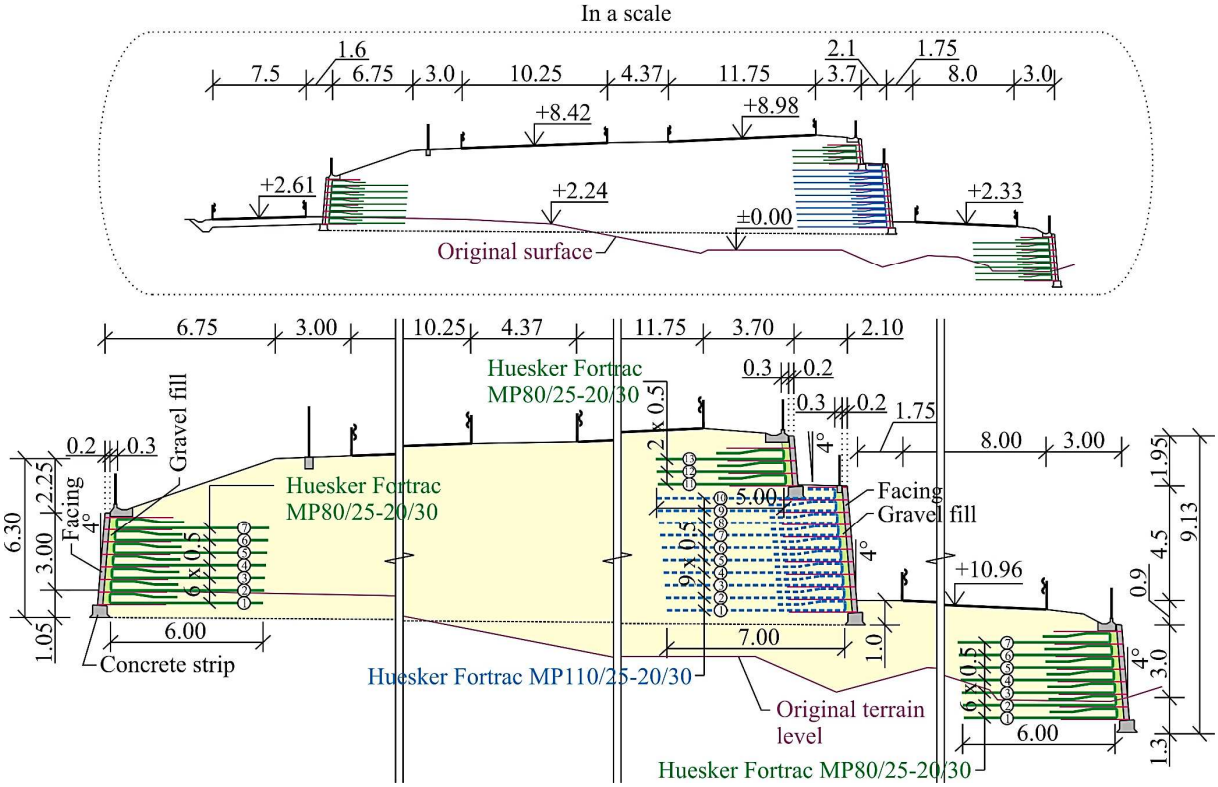


Fig. 1: Cross-section scheme of the reinforced earth embankment - Model 1.

Model 2 represents an embankment for a dual carriageway in a cramped space of a flyover intersection of highways. Because the preliminary design showed insufficient global stability of the embankment, three alternatives with different lengths and placing of geogrids were modelled. In the case of Alternative No. 1, the embankment was supported by wrapped GRS constructed on both sides, which were not connected in any way. MP110/25 geogrids with a length of 8.0 m were used in the lower part, and MP80/25 geogrids with a length of 6.0 m were used in the upper part of the embankment, Fig. 2. In order to increase the stiffness of embankment and improve global stability, 4 independent intermediate geogrids (Thrace TG4040S type) with lengths of 12.0 m (geogrids *c* and *d*), and a length of 14.5 m (geogrids *a* and *b*) were added in Alternative No. 2, Fig. 2. In the case of Alternative No. 3, the stiffness of the embankment is not improved using independent geogrids, but the geogrids Nos. 2, 6, 10, 13, and 16, are designed as continuous and pass from one side of the embankment to other side, Fig. 3. The boundary conditions and loading model are similar to Model 1. In this case, Lane No. 1 was taken into account on the left as well as the right side of the road. The space between them was taken into account as the remaining area. This loading case was assumed as the most critical.

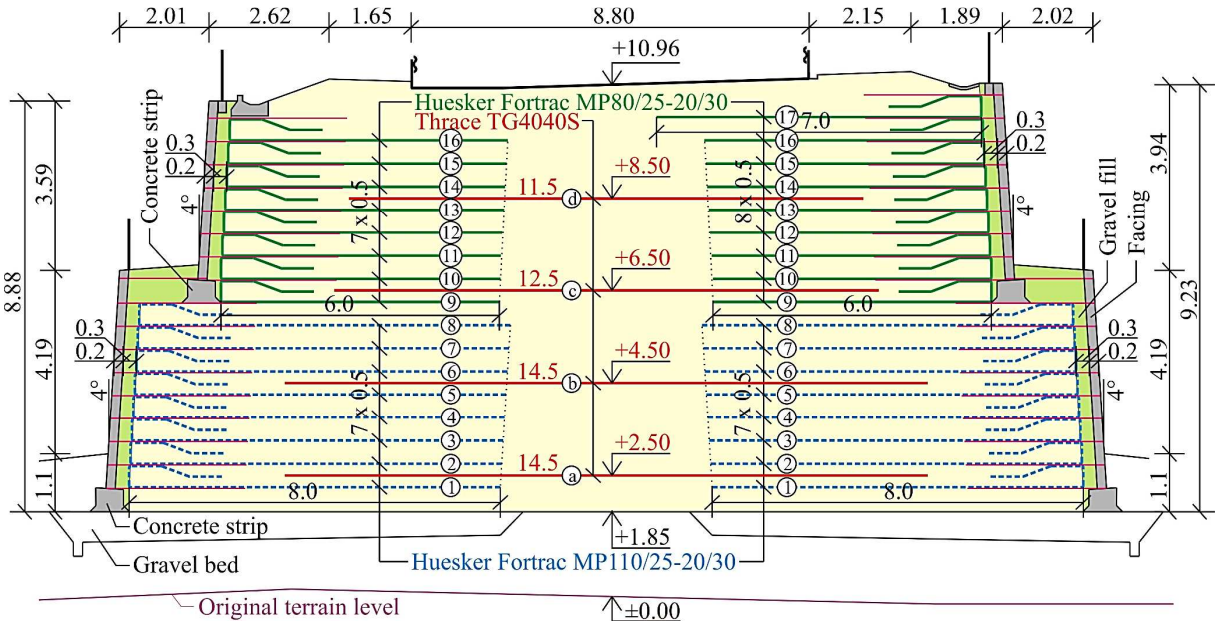


Fig. 2: Cross-section scheme of the reinforced earth embankment - Model 2 (Alternatives Nos. 1 and 2).

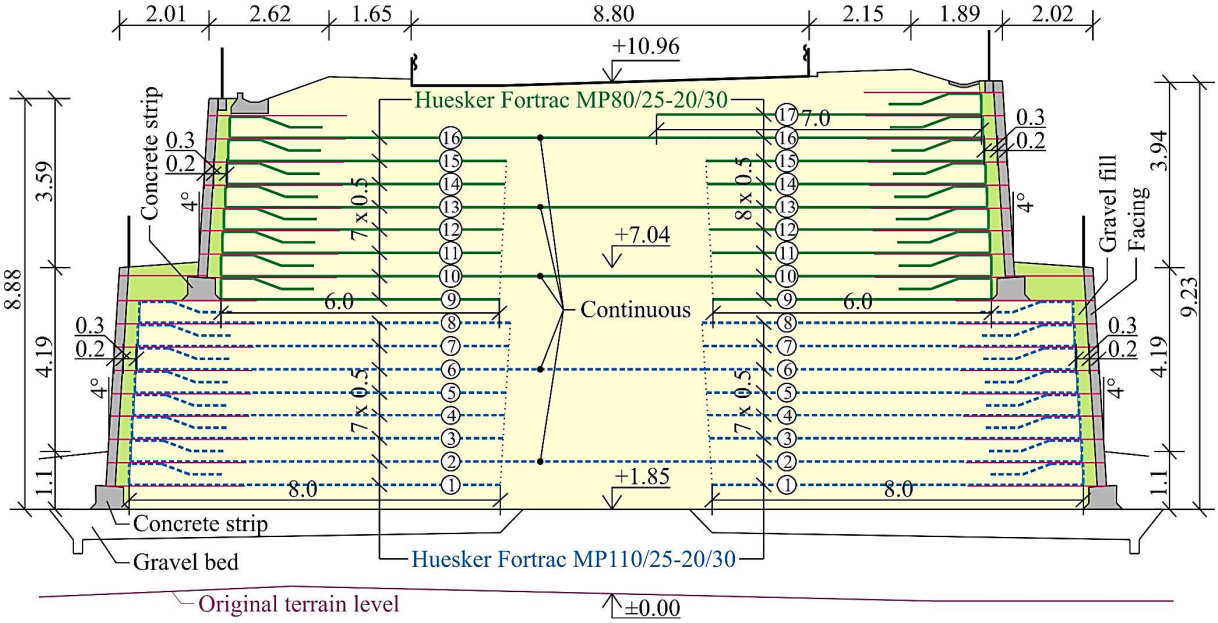


Fig. 3: Cross-section scheme of the reinforced earth embankment - Model 2 (Alternative No. 3).

The preliminary design assumed that the embankment would be built of well graded gravel [25]. In the final design, it was assumed that the embankment would be built of silty gravel, as in the case of Model 1; the properties of the embankment material are presented in Table 4. The subsoil consisted of quaternary fluvial sandy clay and gravel with fine soils to a depth of 8.0 m. Neogene sediments, clay with medium to high plasticity, were located in the continuous layer below the quaternary sediments. Weak rocks to very weak rocks are located below a depth of 9 m from the surface. The groundwater level was about 3.7 m below the terrain level. The properties of facing blocks, gravel poorly graded (used in a space between wrapped GRS and facing blocks), and the concrete strips are presented in Table 1. The properties of soils are presented in Table 4. The construction phases are stated in Table 5.

Table 3: Selected properties of materials for Model 1.

Soil	Embankment		Quaternary					Neogene	
	GM/SM	GP	CI/Y	MS/CS	CI	SF	GF	SC/GC	CI/CH
Parameter (unit)	Gravel silty	Gravel poorly graded	Clay of intermediate plasticity/Fill	Silt/Clay sandy	Clay of intermediate plasticity	Sand with fine content	Gravel with fine content	Sand/ Gravel clayey	Clay of intermediate/ high plasticity
γ[kNm^{-3}]	19	19	20,3	20	20	18,5	19	19,5	19,8
γ_{sat} [kNm^{-3}]	19	19	20,3	20	20	18,5	19	19,5	19,8
$E_{50} = E_{oed}$ [MNm^{-2}]	84	84	11,7	13,06	17,23	59	125	68,6	25,9
E_{ur} [MNm^{-2}]	252	252	46,8	52,24	68,92	177	375	274,4	103,6
m [-]	0,5	0,5	0,7	0,6	0,7	0,5	0,5	0,7	0,7
φ' [°]	28	35	20	24	20	30	35	31	20
ψ' [°]	0	5	0	0	0	0	5	1	0
c' [kNm^{-2}]	5	0	12	12	12	0	0	4	15
k [mday^{-1}]	80	800	0.0015	0.041	0.0024	80	80	0.08	0.015

Table 4: Selected properties of materials for Model 2.

Soil	Embankment		Quaternary		Neogene
	GM/SM	GP	CS/SC	GF	CI/CH
Parameter (unit)	Gravel/Sand silty	Gravel poorly graded	Clay sandy / Sand clayey	Gravel with fine content	Clay of intermediate/high plasticity
γ[kNm^{-3}]	19	19	20	19	19,8
γ_{sat} [kNm^{-3}]	19	19	20	19	19,8
$E_{50} = E_{oed}$ [MNm^{-2}]	84	84	16	120	20
E_{ur} [MNm^{-2}]	252	252	64	360	80
m [-]	0,5	0,5	0,8	0,5	0,7
φ' [°]	28	35	24	35	20
ψ× [°]	0	5	0	5	0
c' [kNm^{-2}]	5	0	10	0	15
k [mday^{-1}]	80	800	0.041	80	0.015

Table 5: Construction phases in the numerical modelling.

Model 1		Model 2 (All alternatives)	
Phase No.	Construction phase	Phase No.	Construction phase
1 - 3	Landscaping - right side	1 - 3	Landscaping
4 - 11	Constructing the wrapped GRS - right side	4 - 20	Constructing the wrapped GRS
12 - 17	Landscaping - left side and middle part	21 - 25	Constructing the passive facing system
18 - 29	Constructing the wrapped GRS - left side and the middle	26	Constructing the pavement
30 - 33	Constructing the passive facing system	27 - 30	Loads from traffic
34 - 35	Constructing the pavement	31 - 34	Stability analysis
36 - 43	Loads from traffic		
44 - 48	Stability analysis		

4 The results obtained

The analysis results include a comparison of tension forces in geogrids and the global stability determined using both calculation methods. The horizontal deformations were determined only by numerical modelling. The numerical analysis includes a comparison of deformations in different construction phases.

4.1 Tension forces in geogrids

The tension forces in geogrid were determined using GEO5 software in the MSE wall module (Analytical model), as well as using the Plaxis software (Numerical model - FEM). The analytical model took into account only the final constructions phase "The embankment is subjected to traffic loads" due to limitations in the software used. The methodology of the calculation is stated in Chapter 3. The results of the numerical modelling are presented for the construction phase "Loads from traffic", Table 5, corresponding to analytical calculation. The characteristic values of the tension forces in geogrids, determined using both methods, are presented in Fig. 4 for Model 1, and Fig. 5 for Model 2 (all alternatives are included).

There is no direct dependence in the differences in tension forces determined using the analytical and numerical model in Model 1, Fig. 4. In the wrapped GRS in the middle of the embankment, the forces in geogrids Nos. 2 - 10 are relatively similar. A significant difference in the forces was obtained in geogrids Nos. 11 - 13, which is caused by different calculation method and boundary conditions, which can be taken into account in the calculations. The differences in the lowest geogrid (No. 1) were significantly different in all wrapped GRS analysed. The analytical model does not take into account the stiffness of the subsoil in any way. In the numerical model, the stiffness of the subsoil and the stiffness of the concrete strip are taken into account, which causes that the force determined by FEM is significantly smaller. A disadvantage of this calculation is that the stiffness of the facing system is not taken into account. In the case of FEM, the forces in the geogrids are significantly affected by the deformation of the embankment. Due to the relatively higher stiffness of the wrapped GRS in the right side, given by dimensions of geogrids, higher terrain in front of the facing of the GRS, and lower lateral earth pressure in the soil, the forces determined by FEM are smaller than forces determined by the analytical model, Fig. 4 - right side. On the contrary, on the left side of the embankment, due to higher loading and lateral earth pressure in the soil, the forces determined by FEM are greater than forces determined by the analytical model, Fig. 4 - left side.

In Model 1, due to the relatively higher stiffness of the embankment and the boundary conditions defined, the forces determined by FEM are smaller than forces determined by the analytical model. The analytical model did not allow defining of intermediate (Alternative No. 2) or continuous geogrids (Alternative No. 3). The difference in forces between each alternative was smaller than a 2 kN/m. Except for the geogrids Nos. 1, 14, 15, and 16, the difference between the forces determined by the FEM and the analytical model were within the range of 11 - 38 %. A significant difference in geogrids Nos. 14, 15, and 16, are caused by different assumptions used in the analytical and FEM calculation, stated in Chapter 3. In numerical modelling, the passive facing system has a minor impact on the values of geogrid forces - the analytical model cannot simulate this. The tension forces in geogrids of pure unloaded wrapped GRS (Phase No. 29) are smaller by about 5 - 30 %.

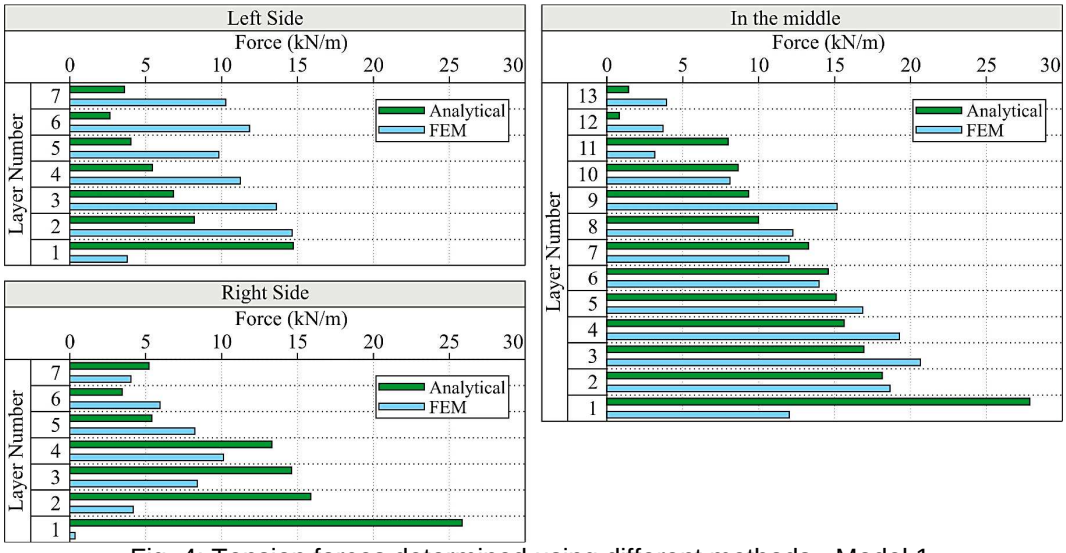


Fig. 4: Tension forces determined using different methods - Model 1.

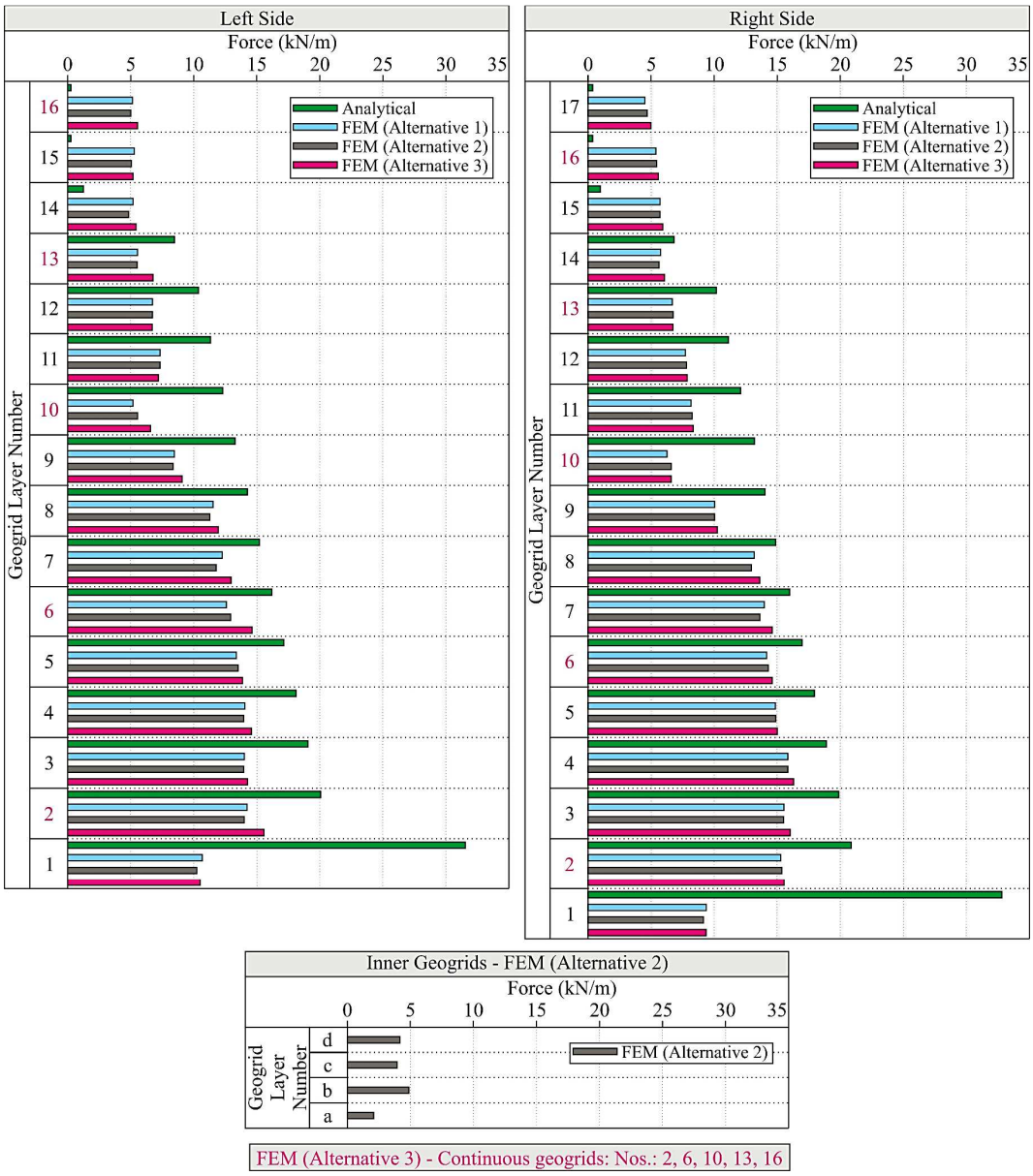


Fig. 5: Tension forces determined using different methods - Model 2.

4.2 Deformations of the reinforced earth structure

In the case of the wrapped GRS with the passive earth system, significant values of horizontal deformations are achieved in three different phases of construction:

- geogrid facing - wrapped GRS constructed to the final height (Model 1 - Phase No. 29; Model 2 - Phase No. 20),
- block facing - deformation of the passive facing system constructed to the total height (Model 1 - Phase No. 35; Model 2 - Phase No. 26),
- block facing - deformation of the passive facing system, when the load from traffic is taken into account (Model 1 - Phase No. 43; Model 2 - Phase No. 30).

The horizontal deformations for phase No. 29 in Model 1 are plotted in Fig. 6. The greatest value of the horizontal deformation of the wrapped GRS body reaches 96 mm. During the construction of a passive facing system, this deformation is compensated by compacted gravel in a space between the wrapped GRS body and facings blocks. Due to this reason, the horizontal deformation of the blocks facing is significantly smaller. The maximum horizontal deformation of the passive facing system in phase No. 43 is less than 14 mm, Fig. 7.

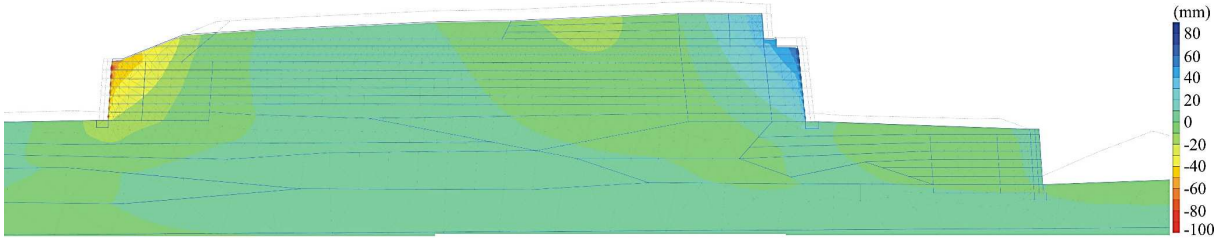


Fig. 6: Horizontal deformations of the reinforced earth embankment in phase No. 29 - Model 1.

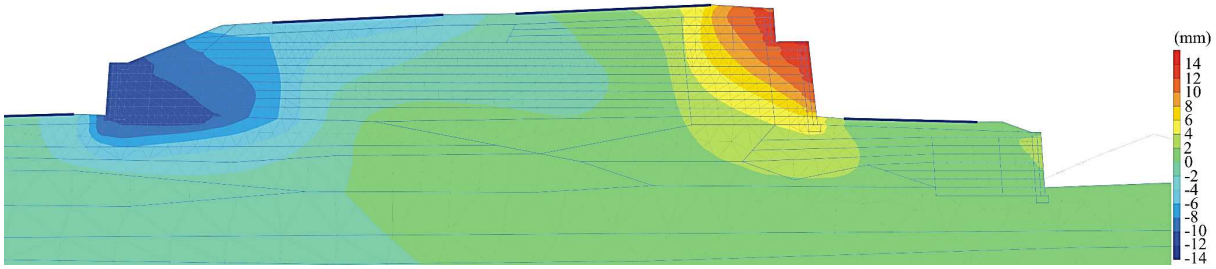


Fig. 7: Horizontal deformations of the reinforced earth embankment in phase No. 43 - Model 1.

The horizontal deformations of geogrid facing or blocks facing, according to the adequate construction phase, for Model 2, are presented in Fig. 8 for the lower part of the embankment (geogrids Nos. 1 - 8), and Fig. 9 for the upper part of the embankment (geogrids Nos. 9 - 16, or geogrids Nos. 9 - 17, respectively). In the upper part of the embankment, the horizontal deformation of the block facing (in phase No. 26 - without the loading) is lower by 2.8 ~ 3.3-times than the horizontal deformation of the pure wrapped GRS body, which occurs during the construction (phase No. 20). In the lower part of the embankment, the horizontal deformations in phase No. 26 is lower for 3.6 ~ 3.8-times than the horizontal deformation in phase No. 20. Considering traffic load, the horizontal deformation of the facing block increases from about 11.0 mm to 14.8 mm (left side), and 17.0 mm (right side), respectively. Similar differences between each phase were also obtained in the lower part of the embankment, see Fig. 9.

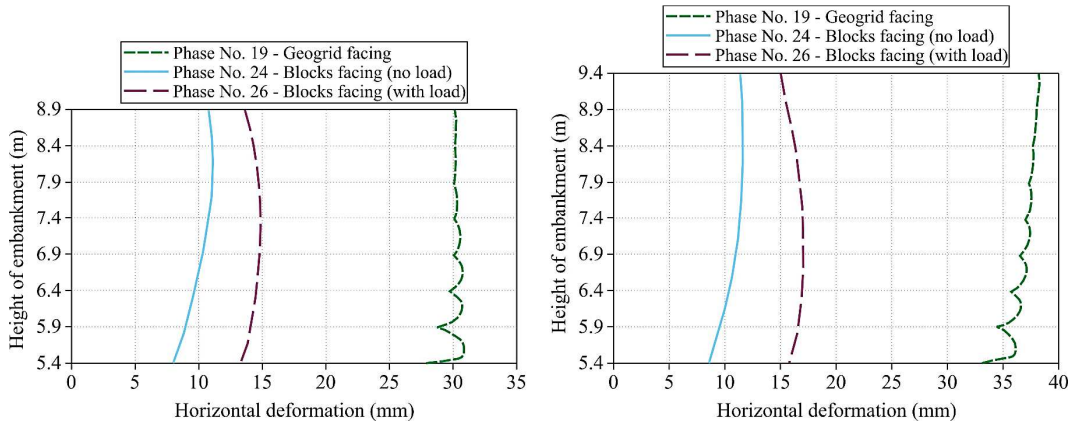


Fig. 8: Horizontal deformations of the upper part of the embankment facings in different phases - Model 2, Alternative No. 3.

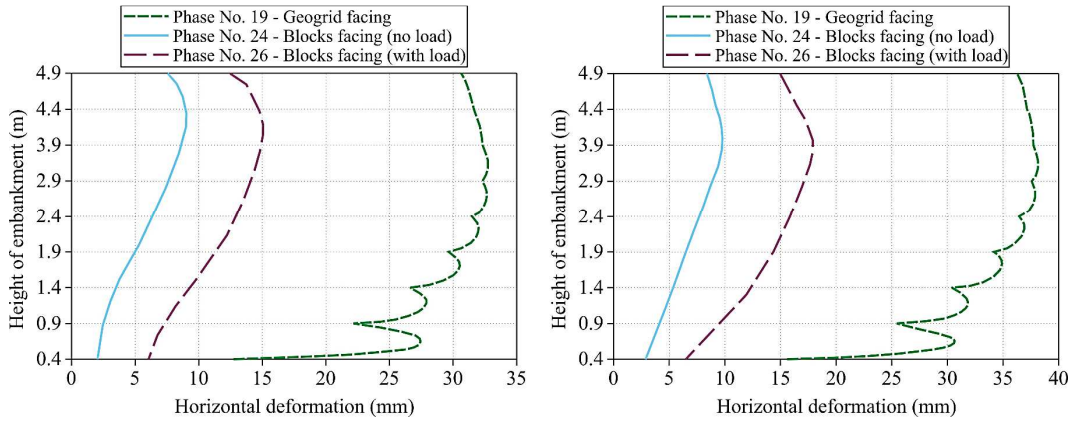


Fig. 9: Horizontal deformations of the lower part of the embankment facings in different phases - Model 2, Alternative No. 3

4.3 Global stability of the reinforced earth structure

Global stability was determined using both methods, i.e., the analytical model (GEO5 software - global stability module) and FEM. GEO5 software - global stability module allowed for modelling the whole embankment. The intermediate geogrids in Alternative No. 2 and continuous geogrids in Alternative No. 3 were also modelled. The analytical model did not allow for modelling the facing system; however, the facing stiffness has a minor effect on global stability. In the case of the numerical modelling, all parameters, such as stiffness of geogrids, stiffness of the pavement, and stiffness of the facing system, affect the final shape of the slip area. Due to this reason, the shape of the sliding area determined by FEM can be considered more accurate.

The results of the safety analysis of Model 1 are presented in Fig. 10. On the left side of the embankment, the lowest value of the safety factor was determined using FEM. On the contrary, on the right side of the embankment, the lowest value of the safety factor was determined using an analytical calculation based on Sarma's method. Both analytical models also allowed for determining individual sliding areas for the GRS in the middle of the embankment as well as for the GRS on the right side of the embankment. The difference between the safety factors determined using different methods is about 22 %. All the safety factors determined using different methods exceeded the required value of 1.50.

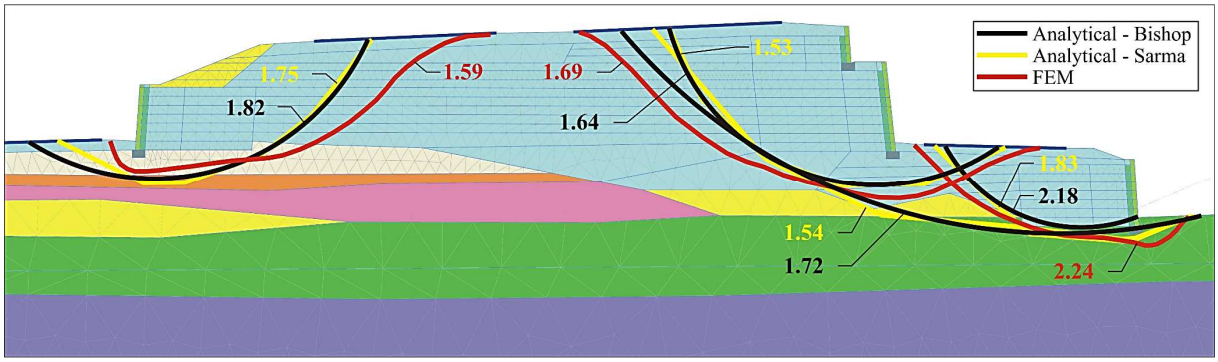


Fig. 10: Sliding areas determined using different methods - Model 1.

In the case of Model 2, all alternatives are presented separately. The results for Alternative No. 1 are shown in Fig. 11, and the results for Alternative No. 2 are shown in Fig. 12. The results for Alternative No. 3 are shown in Fig. 13. The analytical methods were determined individually for the left and right side of the embankment. The results of the numerical modelling showed that the embankment could collapse concurrently to both sides. This effect causes that the lowest value of the safety factor was determined using numerical modelling. In the case of Alternative 1, the values of the safety factors determined using the FEM and Sarma's method were lower than the required 1.50. It was evaluated that the global stability is not fulfilled. For this reason, Alternatives Nos. 2 and 3 have been created and analysed. In both cases, the safety factor determined using all methods exceeded the required value of 1.50. In general, the highest values of the safety factor were reached in

Alternative No. 3, where the continuous geogrids Nos. 2, 6, 10, 13, and 16 are designed. This alternative was also used in the practice because it has been assumed that placing the continuous geogrids is more accessible and less time-consuming than the placing of intermediate geogrids (Alternative 2).

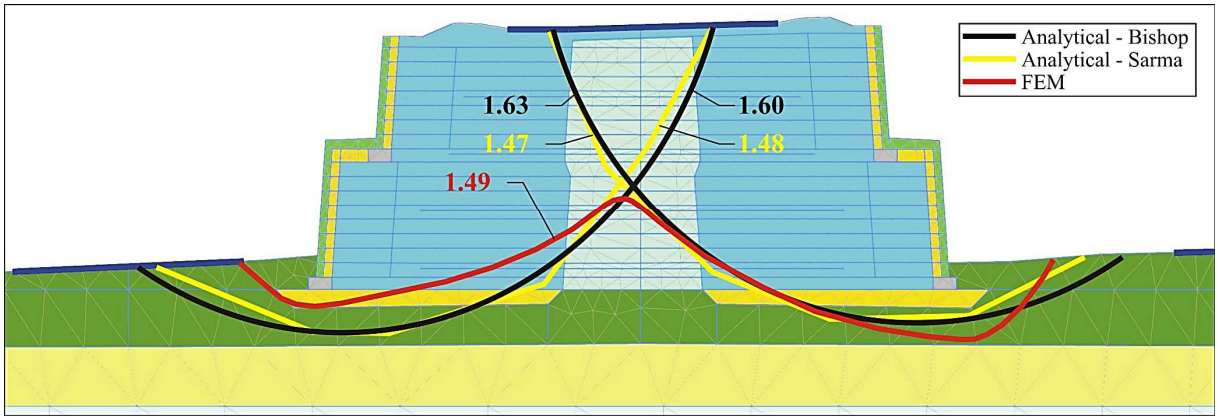


Fig. 11: Sliding areas determined using different methods - Model 2, Alternative 1.

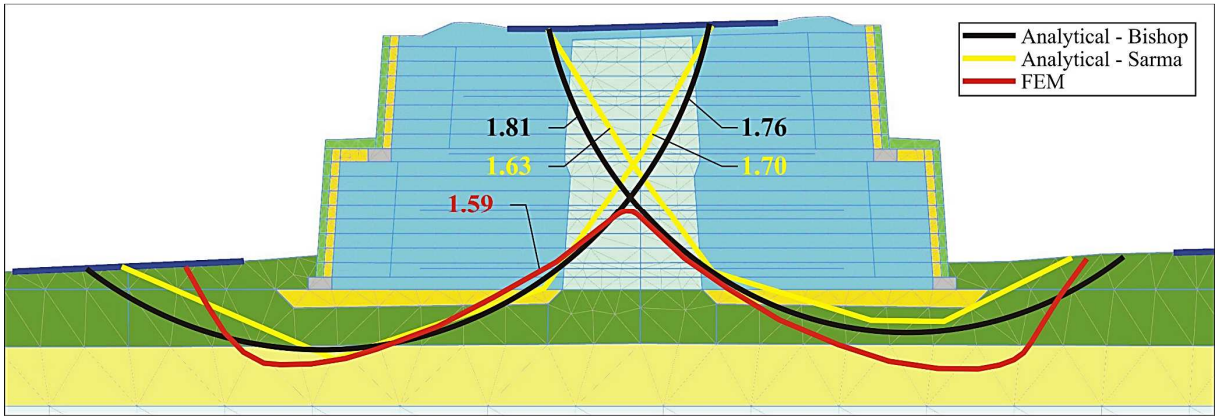


Fig. 12: Sliding areas determined using different methods - Model 2, Alternative 2.

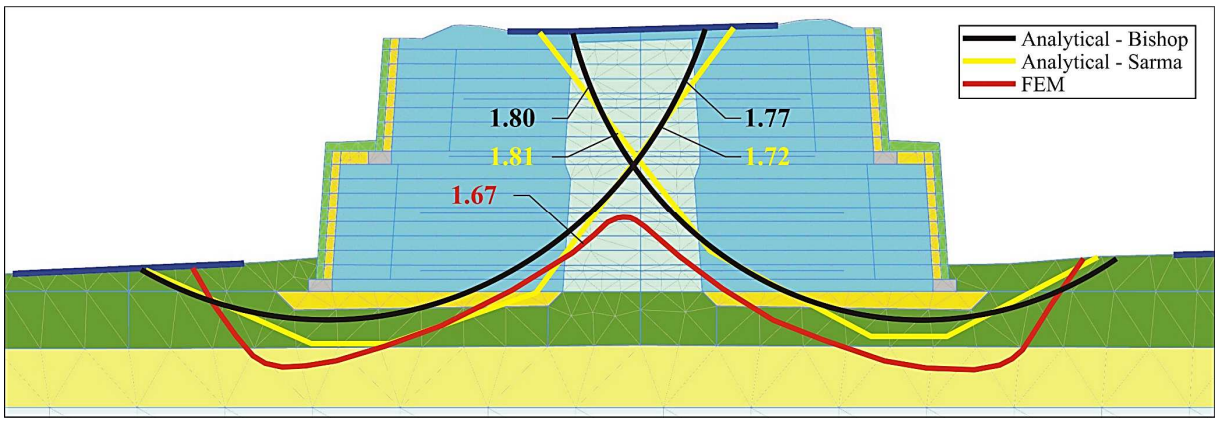


Fig. 13: Sliding areas determined using different methods - Model 2, Alternative 3.

5 Conclusion

The article presents an analysis of road embankments for two selected complex cross-sections marked Model 1 and Model 2 in the study. The sides of the embankments are supported by a wrapped geogrid retaining structure (GRS) with a passive facing system. In this technology, the main body of the embankment, supported by the wrapped GRS, is built to a total height in the first step. Subsequently, the passive facing system, which consists of facing blocks and compacted gravel between the facing and the wrapped GRS, is constructed. The road embankment in Model 1 is

supported by three wrapped GRS, which not affect each other. In the case of Model 2, the wrapped GRS at both sides of the embankment can significantly affect each other.

The analytical calculations were done using the FINE Geo 5 geotechnical software, and numerical modelling, based on the finite element method (FEM), was done using Plaxis geotechnical software. The forces in geogrids, determined using both software, were more or less different from each other. The analytical calculations were based on a simple method and allowed to take into account only simplified boundary conditions. The numerical modelling allowed considering more precise boundary conditions, such as, e.g., stiffness of the passive facing system or the concrete strips below the side of the embankment. Due to difficult boundary conditions, it was impossible to determine any direct dependence between the forces determined using both software.

The numerical modelling showed that the deformation of the wrapped GRS, which occurs during the construction, is about 2.8 - 3.8 times greater than the final deformation of the unloaded embankment and about 2.1 - 2.2 times greater than the final deformation of the loaded embankment.

In Model 1, the safety factors were within the range of 1.59 - 1.82 for the left side of the embankment and 1.53 - 2.24 for the right side of the embankment. The required value of 1.5 was exceeded using all calculation methods. In the case of Model 2, the numerical modelling results showed that the embankment could collapse concurrently to both sides. Due to this reason, three alternatives of geogrid placing were analysed. The stability analysis results showed that placing intermediate or continuous geogrids, which connect the GRS at the left and right side of the embankment, is necessary to obtain a safety factor greater than 1.5.

The study results showed that the numerical modelling is more suitable for the design of embankment supported by the wrapped GRS with the passive facing system because it allowed for a more accurate consideration of complex boundary conditions.

Acknowledgements

The project presented in this article is supported by the VEGA Grant No. 1/0530/19.

References

[1] ALLEN, T. M. - BARTHUS, R. J.: Design and Performance of 6.3 m High, Block-Faced Geogrid Wall Designed Using K-Stiffness Method. Journal of Geotechnical and Geoenvironmental Engineering, Vol. 140, Iss. 2, 2014, p. 12, https://doi.org/10.1061/(ASCE)GT.1943-5606.0001013.

[2] DOLINAJOVA, K. - SNAHNICAN, J.: Geogrid and Double Twist Steel Mesh Reinforced Soil Walls Subjected to High Loads in a Seismic Area. Proceedings of the 12th Slovak Geotechnical Conference: 55 Years of Geotechnical Engineering in Slovakia, 1st-2nd June, 2015, Bratislava, Slovakia, 2015, pp. 79-87.

[3] SCOTLAND, I. - DIXON, N. - FROST, M. - WACKROW, R. - FOWMES, G. - HORGAN, G.: Measuring Deformation Performance of Geogrid Reinforced Structures Using a Terrestrial Laser Scanner. Proceedings of 10th International Conference of Geosynthetics, September 2014, Berlin, Germany, 2014, p. 8, https://www.researchgate.net/publication/286860094_Measuring_deformation_performance_of_geogrid_reinforced_structures_using_a_terrestrial_laser_scanner.

[4] SILBER-HASSLACHER, T. - SNAHNICAN, J.: Active and Passive Facing Systems for Reinforced Soil Structures. 13th Geosynthetics Annual Conference 2019, 7-8. February, 2019, Zilina, Slovakia, 2019, p. 9, http://www.geosoul.sk/wp-content/uploads/2019/02/GEOSYNTETIKA2019_ACTIVE-AND-PASSIVE-FACING-SYSTEMS-FOR-REINFORCED-SOIL-STRUCTURES.pdf.

[5] BUSSERT, F. - CAVANAUGH, J.: Recent Research and Future Implications of the Actual Behaviour of Geogrids in Reinforced Soil. Proceedings of Earth Retention Conference 3, August 2010, Washington, USA, 2010, pp. 460-477, https://doi.org/10.1061/41128(384)46.

[6] BARNES, G.E.: Soil Mechanics: Principles and Practice. 3rd edition, London: Palgrave, UK, 2010, p. 560.

[7] ALLEN, T. M. - BATHURST, R. J.: Observed Long-term Performance of Geosynthetic Walls and Implications for Design. Geosynthetics International, Vol. 9, Iss. 5-6, 2002, pp. 567-606, https://doi.org/10.1680/gein.9.0228.

[8] ALLEN, T. - BATHURST, R. J.: An Improved Simplified Method for Prediction of Loads in Reinforced Soil Walls. Journal of Geotechnical and Geoenvironmental Engineering, Vol. 141, Iss. 11, 2015, p. 14, https://doi.org/10.1061/(ASCE)GT.1943-5606.0001355.

[9] WU, J. T. H.: CTI-UCD-1-94: Design and Construction of Low Cost Retaining Walls: The Next Generation in Technology. Colorado Transport Institute, Denver, Colorado, USA, 1994, p. 152, https://www.codot.gov/programs/research/pdfs/1994-research-reports/retainingwalls.pdf.

[10] HRLICH, M. - MIRMORADI, S. H.: Evaluation of the Effects of Facing Stiffness and Toe Resistance on the Behavior of GRS walls. Geotextiles and Geomembranes, Vol. 40, 2013, pp. 28-36, https://doi.org/10.1016/j.geotexmem.2013.07.012.
[11] DRUSA, M. - VLCEK, J.: Importance of Results Obtained from Geotechnical Monitoring for Evaluation of Reinforced Soil Structure - Case Study. Journal of Applied Engineering Sciences, Vol. 6, Iss. 1, 2016, pp. 23-27, https://doi.org/10.1515/jaes-2016-0002.
[12] WANG, Z. - JACOBS, F. - ZIEGLER, M.: Visualization of Load Transfer Behaviour between Geogrid and Sand Using PFC2D. Geotextiles and Geomembranes, Vol. 42, Iss. 1, 2014, pp. 83-90, https://doi.org/10.1016/j.geotexmem.2014.01.001.
[13] YASHIMA, A. - TSUJI, S. - YOSHIDA, K. - YOKOTA, Y.: A New Optical Fibre Sensor to Assess the Stability of Geogrid-reinforced Soil Walls. Geosynthetics International, Vol. 16, Iss. 4, 2009, pp. 238-245, https://doi.org/10.1680/gein.2009.16.4.238.
[14] BENJAMIM, C. V. S. - ZORNBERG, J. G. - BUENO, B. S.: Field Monitoring Evaluation of Geotextile-Reinforced Soil-retaining Walls. Geosynthetic International, Vol. 14, Iss. 2, 2007, pp. 100-118, https://doi.org/10.1680/gein.2007.14.2.100.
[15] LEE, Y. B. - KO, H. Y. - MCCARTNEY, J. S.: Deformation Response of Shored MSE Walls under Surcharge Loading in the Centrifuge. Geosynthetics International, Vol. 17, Iss. 6, 2010, pp. 389-402, https://doi.org/10.1680/gein.2010.17.6.389.
[16] EHRLICH, M. - MIRMORADI, S. H. - SARAMAGO, R. P.: Evaluation of the Effects of Compaction on the Behavior of Geosynthetic-reinforced Soil Walls. Geotextiles and Geomembranes, Vol. 34, 2012, p. 108-115, https://doi.org/10.1016/j.geotexmem.2012.05.005.
[17] SCOTLAND, I. - DIXON, N. - FROST, M. - FOWMES, G. - HORGAN, G.: Modelling Deformation During the Construction of Wrapped Geogrid Reinforced Structures. Geosynthetics International, Vol. 23, Iss. 3, 2016, pp. 219-232, https://doi.org/10.1680/jgein.15.00049.
[18] FINE GEO5 - User Guide 3/2021. https://www.finesoftware.eu/user-guides/.
[19] NGUYEN, G.: Determination of Stress in Spread Foundation Subsoil by Various Approaches. Civil and Environmental Engineering, Vol. 11, Iss. 1, 2015, pp. 28-36, https://doi.org/10.1515/cee-2015-0004.
[20] PLAXIS 2D CE V21.01:1 - Tutorial Manual, https://communities.bentley.com/products/geotech-analysis/w/plaxis-soilvision-wiki/46137/manuals---plaxis.
[21] SCHANZ, T. - VERMEER, P. A. - BONNIER, P. G.: The Hardening Soil Model: Formulation and Verification. In: Beyound 2000 in Computational Geotechnics – 10 Years of Plaxis, International Symposium, Amsterdam, Netherlands, 1999, pp. 281-296, https://doi.org/10.1201/9781315138206-27.
[22] MIRMORADI, S. H. - EHRLICH, M.: Modeling of the Compaction-induced Stress on Reinforced Soil Walls. Geotextiles and Geomembranes, Vol. 43, Iss. 1, 2015, pp. 82-88, https://doi.org/10.1016/j.geotexmem.2014.11.001.
[23] DRUSA, M. - VLCEK, J. - HOLICKOVA, M. - KAIS, L.: Analytical and Numerical Evaluation of Limit States of MSE Wall Structure. Civil and Environmental Engineering, Vol. 12, Iss. 2, 2016, pp. 145-152, https://doi.org/10.1515/cee-2016-0020.
[24] STACHO, J. - SULOVSKA, M. - SLAVIK, I.: Determining the Shear Strength Properties of a Soil-geogrid Interface Using a Large-scale Direct Shear Test Apparatus. Periodica Polytechnica Civil Engineering, Vol. 64, Iss. 4, 2020, pp. 989-998, https://doi.org/10.3311/PPci.15766.
[25] SULOVSKA, M. - STACHO, J.: Design of Road Embankment Reinforced Using a Geogrid. SGEM 2019. 19th International Multidisciplinary Scientific GeoConference. Vol. 19. Science and Technologies in Geology, Exploration and Mining, Sofia, Bulgaria, 2019, pp. 145-152, https://doi.org/10.5593/sgem2019/5.4/S22.047.